Ring dark solitary waves: Experiment versus theory

A. Dreischuh,[1] D. Neshev,[1,2] G. G. Paulus,[3] F. Grasbon,[3] and H. Walther[3,4]
[1] *Department of Quantum Electronics, Sofia University, 5 J. Bourchier Boulevard, BG-1164 Sofia, Bulgaria*
[2]*Nonlinear Physics Group, RSPhysSE, The Australian National University, 0200 ACT Canberra, Australia*
[3]*Max-Planck-Institut für Quantenoptik, Hans-Kopfermann-Straße 1, D-85748 Garching, Germany*
[4]*Sektion Physik, Ludwig-Maximilians-Universität, Am Coulombwall 1, D-85747 Garching, Germany*
(Received 10 September 2002; published 26 December 2002)

Experimental results on optical ring dark solitary wave dynamics are presented, emphasizing the interplay between initial dark beam contrast, total phase shift, background-beam intensity, and saturation of the nonlinearity. The results are found to confirm qualitatively the existing analytical theory and are in agreement with the numerical simulations carried out.

DOI: 10.1103/PhysRevE.66.066611 PACS number(s): 42.65.Tg, 42.65.Jx

I. INTRODUCTION

Optical dark spatial solitons (DSSs) are exact solutions of the nonlinear Schrödinger equation (NLSE) for defocussing nonlinearity and nonvanishing boundary conditions [1]. Physically, they form on background beams of finite width as self-supported intensity dips due to the counterbalance between beam self-defocussing and diffraction. The required defocussing nonlinearity of the medium causes an inevitable reduction of the beam intensity. Losses, saturation, and high transverse dimensionality result in nonintegrable model equations. Despite certain adiabatic relaxation characteristics, the solitary solutions of these equations have a large number of characteristics [2] in common with the soliton solution of the one-dimensional NLSE and are widely denoted by the term ''dark soliton.'' DSSs were generated as dark stripes [3,4], whereas the only known truly two-dimensional optical DSS is the optical vortex soliton (OVS) [5]. Characteristic of the phase portraits of these beams are an one-dimensional π-phase jump and an on-axis 2π helical phase ramp, also denoted as edge-phase and screw-phase dislocations, respectively.

A special class of DSSs are the optical ring dark solitary waves (RDSWs). They were first introduced by Kivshar and Yang [6] as a two-dimensional nonstationary solution of the NLSE. Their evolution was studied in the frame of the adiabatic approximation of perturbation theory. The quasi-one-dimensional treatment allowed the authors to obtain an expression for the RDSW's transverse velocity as a function of the ring radius and contrast. In addition, a linear stability analysis was performed. The authors showed that in the small-amplitude limit these ring dark waves are described by the cylindrical Korteweg-de Vries equation, which has ring soliton solutions [6]. Recently, Frantzeskakis and Malomed derived new equations of evolution for small-amplitude solitary waves on a finite background [7] by means of a multiscale expansion method applied to the generalized cylindrical NLSE. Their long-wave solitary solutions propagate ''on top'' of the continuous-wave background as a dark perturbation in Kerr defocussing media. Depending on the background-beam intensity, they can appear both dark and antidark for Kerr-like saturable defocussing nonlinearity.

The RDSWs may turn out to be of a practical interest because of their ability to induce waveguides in which multiple signal beams could be guided in parallel [8]. Therefore, a detailed analysis of the dynamics of these solitary structures is required. The first experimental generation of optical RDSWs [9] was conducted with pure amplitude modulation (metal micrometer-sized dot reflecting part of the laser beam) at the front of the nonlinear medium (NLM). Under such conditions, a ring dark formation was observed and pairs of phase jumps oppositely shifted by about $\pi/2$ were measured in each diametrical slice of the RDSWs [10]. In a subsequent experiment [11], RDSWs were generated from odd initial conditions by using binary computer-generated holograms (CGHs) [12]. Inside a circle the phase was shifted by π vs the outlying area by shifting the photolithographically produced interference lines by half a grating period. In both experiments the phase profiles were measured by multiple-frame interferometric technique for optical wave front reconstruction [13]. It was found that, along the NLM, the transverse velocity of the RDSWs born from even initial conditions is higher than that of the odd ones. Additionally, the transverse velocity is higher for rings with smaller initial radii [11]. Numerical simulations have shown that, besides the ring radius, the transverse velocity of the RDSW can be effectively controlled by initial phase modulation of the background beam (inside, outside or on both sides of the phase dislocation) or by nonlinear interaction with a second coaxial dark formation (RDSW or OVS) [14]. In saturable media, the RDSW's transverse velocity is lower than that in Kerr NLM. At high saturation levels, in formal contradiction to but in actual agreement with the one-dimensional case, decay of the dark rings into a loop of optical vortices of alternating helicities should be expected [15].

In the present paper we investigate experimentally the dynamics of the RDSWs taking into account all the different parameters for controlling the initial conditions. The results are compared with the predictions of the analytical description and numerical data. In particular, we analyzed the nonmonotonic transverse dynamics of RDSWs in a saturable NLM as a function of the background-beam intensity and nonlinear propagation. Additionally, the influence of the total phase shift encoded in the CGHs was investigated. It was found that it affects the dynamic of the dark rings even in the free-space propagation from the CGH to the entrance of the

NLM. Inside the NLM the RDSWs experience monotonic or nonmonotonic dynamic depending on the phase shift. These experimental findings verified the analytical predictions of Kivshar and Yang [6].

II. THEORETICAL MODEL

The transverse evolution of the RDSWs in bulk homogeneous, isotropic, and saturable NLM is described by the generalized NLSE for the slowly varying envelope of the electric field,

$$i\frac{\partial E}{\partial z}+\frac{1}{2}\Delta_{\perp}E-\frac{L_{Diff}}{L_{NL}}f(I)E=0, \tag{1}$$

where $I=|E|^2$ is beam intensity expressed in units of the intensity I_{sol}^{1D} needed to generate one-dimensional dark soliton of a width r_0. The initial width of the RDSW is chosen equal to r_0, and $\Delta_{\perp}=\partial^2/\partial\xi^2+\partial^2/\partial\eta^2$ is the transverse Laplacian. The transverse spatial coordinates are normalized to r_0 ($\xi=x/r_0$, $\eta=y/r_0$), and the nonlinear propagation path length z is expressed in units of Rayleigh diffraction lengths $L_{Diff}=kr_0^2$. Furthermore, $L_{NL}=(k|n_2|I_{sol}^{1D})^{-1}$ is the nonlinear length in a Kerr medium and k is the wavenumber inside the NLM. For soliton propagation $L_{NL}=L_{Diff}$. The function $f(I)$ is used to describe the response of the NLM,

$$f(I)=\begin{cases} I & \text{Kerr type,}\\ I-qI^2 & \text{cubic-quintic type [16],}\\ 1-1/(1+sI) & \text{two-level medium [17],}\\ I/(1+sI)^{\gamma} & \text{phenomenological.}\end{cases} \tag{2}$$

The analytical results in Ref. [6] were obtained for Kerr-type nonlinearity and the dark ring was considered as an exact dark soliton stripe solution bent in a circle of radius $R(z)$,

$$E(r,z)=E_0[\cos\phi(z)\tanh\Theta+i\sin\phi(z)]e^{-iI_0z}, \tag{3}$$

$$\Theta=E_0\cos\phi(z)[r-R(z)], \tag{4}$$

where $\phi(z)$ ($|\phi|<\pi/2$) is the slowly varying RDSW angle. The soliton angle is related to the total phase shift across the ring $\Delta\Phi(z)=\Phi_{in}-\Phi_{out}=\sigma[2\phi(z)-\pi]$ ($|\Delta\Phi|<\pi$), where $\sigma=\mathrm{sgn}\,\phi(z)$. The intensity contrast of the RDSW $A^2(z)=(I_0-I_{min})/I_0$ satisfy the relation

$$\Delta\Phi(z)=2\arcsin(A), \tag{5}$$

$I_0=E_0^2$ is the background-beam intensity, and I_{min} is the minimum intensity in the RDSW.

For large values of the soliton radius, the RDSW can be regarded as quasi-one-dimensional object with a curvature treated as a perturbation. In this adiabatic approximation one can obtain an expression for the dark ring radial velocity $v=dR/dz$ as a function of the initial ring radius $R_0=R(z=0)$ and the initial total radial phase shift $\Delta\Phi_0=\Delta\Phi(z=0)$ [6],

$$v=\sigma(0)E_0\left[1-\sin^2(\Delta\Phi_0/2)\left(\frac{R_0}{R(z)}\right)^{2/3}\right]^{1/2}. \tag{6}$$

Equation (6) shows the existence of a minimal radius of the RDSW,

$$R_{min}=R_0[\sin(|\Delta\Phi_0|/2)]^3,\quad \Delta\Phi_0<0, \tag{7}$$

at which the RDSW has maximal contrast.

Equations (6) and (7) carry a simple physical meaning: The initial dark ring exhibits monotonic increase of its radius if the phase inside the ring is higher than the phase outside ($0<\Delta\Phi_0\leqslant\pi$). In the opposite case ($-\pi<\Delta\Phi_0<0$) the radius of the RDSW first decreases to its minimal value R_{min} and monotonically increases afterwards. The decrease of the ring radius is related to an increase of its contrast and the other way around.

The above results cannot be easily generalized for the model of the saturable nonlinearity, but an idea for the influence of the saturation could be found applying the particular case of competitive cubic-quintic nonlinearity [Eq. (2), second model, $q>0$]. In this case the result for the total phase shift, analogous to Eq. (5), is given by [16]

$$\Delta\Phi=2\arcsin\left(\frac{A}{A^2+c(1-A^2)}\right), \tag{8}$$

where the coefficient c is

$$c=\frac{1+2qI_0(4-A^2)/3}{1+2qI_0(1-A^2)/3}. \tag{9}$$

A relation for the transverse velocity cannot be found analytically, however, in the context of the approximations used by Kivshar and Yang [6], a good description could be obtained by the relation

$$v(z)=\sigma E_0\cos(\Delta\Phi(z)/2), \tag{10}$$

where the total phase shift $\Delta\Phi(z)$ is given by Eqs. (8) and (9). The above relation appears useful if one can measure the intensity contrast of the dark ring at different propagation distances.

For the numerical description of the RDSW dynamics we used the phenomenological model for saturable nonlinearity in Eq. (2), with parameters s and γ fitted to match the real experimental conditions. In all the numerical calculations the RDSW [Eqs. (3) and (4)] is superimposed on a finite background super-Gaussian beam $B(r)=\exp[-(\sqrt{r^2/w^2})^{14}]$. In order to avoid any influence of the finite background, the width w was chosen to exceed at least five times the initial RDSW radius R_0.

III. RDSW TRANSVERSE VELOCITY VS INTENSITY

A. The experimental model of the nonlinearity

The experimental setup is shown in Fig. 1(a). In order to obtain a dark ring of a desired radius and a phase jump of a certain magnitude, a single-line Ar^+ laser ($\lambda=488$ nm) is

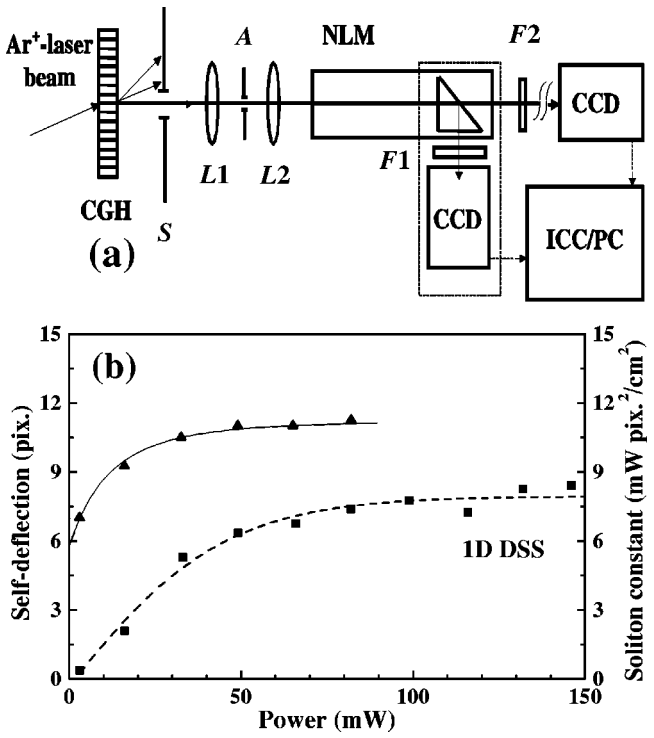

FIG. 1. (a) Experimental setup: CGH, computer-generated hologram; S, slit; A, aperture; $L1$ and $L2$, AR-coated lenses ($f=80$ mm); NLM, $F1$, $F2$, filter sets, CCD camera with 13 μm resolution; ICC/PC, personal computer equipped with an image-capturing card. (b) Power dependences of the background-beam self-deflection (triangles) and of the quantity $I_0 r_0^2$ (squares) indicating $P_{sat} \approx 35$ mW and $P_{sol}^{1D} \approx 90$ mW. Solid (dashed) curve, sigmoidal fits.

used to reconstruct the respective CGH. The latter are produced photolithographically with a grating period of 18 μm and ensure a diffraction efficiency of nearly 10% in first order. The dark rings are generated in the ± 1 diffraction order of a CGH, whereas the sign of the phase jump in the $+1$ order is opposite to the sign in the -1 order. The laser beam, diffracted in first order with the dark ring nested in, is transmitted through a slit placed about 15 cm behind the CGH and is gently focused on the entrance of the NLM. The nonlinear medium is ethylene glycol dyed with DODCI (diethyloxadicarbocyanine iodine). After passing the desired nonlinear propagation path length (0.5 cm–8.5 cm) the dark beam is partially reflected by a prism immersed in the liquid and is projected directly on a comoving charge-coupled device (CCD) camera with a resolution of 13 μm. Alternatively, the dark beam can be recorded at the exit of the NLM. For further evaluation the images are stored by an image-capturing system.

To obtain the exact function of the nonlinear response of the NLM, two calibration experiments were performed. The data presented below refer to an absorption of $\alpha = 0.107\ \mathrm{cm}^{-1}$ at $\lambda = 488$ nm. In the first calibration measurement we generated a dark soliton stripe by using a CGH of the respective type. The soliton constant $I_0 r_0^2$ (i.e., the product of the background-beam intensity and the square of the dark beam width measured at the $1/e^2$ level) was measured and it was found to reach its asymptotically constant value for input powers $P_{sol}^{1D} \approx 90$ mW [Fig. 1(b), dashed curve]. In a second calibration experiment we realized a beam self-bending scheme, similar to the one used in Ref. [18]. The required asymmetry was introduced by tilting the prism immersed in the NLM. This asymmetry results in different propagation path lengths for the different parts of the beam. The strength of the self-bending effect [Fig. 1(b), solid curve], measured in the near field, gives the actual form of the nonlinear response, which is saturable with an estimated saturation power $P_{sat} \approx 35$ mW. To match the exact function we used the phenomenological model in Eq. (2) and obtained the values for the fitting parameter s and γ. In all the cases $\gamma \approx 3$, while the value for s was different depending of the concentration of the dye in the liquid. For the example presented in Fig. 1(b), the value of $s = P_{sol}^{1D}/P_{sat} = 2.6$. Other solutions with different concentration of the dye were measured where $s = 0.4; 0.6;$ and 1.4.

B. Intensity dependence of the transverse dynamics

When a RDSW is generated by pure amplitude modulation of the background beam at the entrance of the NLM, its transverse velocity increases monotonically with the intensity (up to $2.5 P_{sol}^{1D}$; see Fig. 7 in Ref. [9]). When CGH is used to generate a black ring (with π phase jump), we observe a nonmonotonic change of the ring radius vs background beam power for a nonlinear propagation length of $z = 8.5$ cm [Fig. 2(a)]. An evident minimum is observed for a power slightly below P_{sol}^{1D}. The corresponding data for the contrast of the RDSW show reversed nonmonotonic behavior [Fig. 2(b), solid curve]. For the power at which the dark ring has a minimum radius, the contrast is maximal. Generally, this is consistent with the theory [Eqs. (6) and (7)], showing that the decrease of the beam diameter leads to higher contrast of the solitary wave and correspondingly higher total phase shift. As will be discussed later (see Fig. 4, the shaded region), the dark rings generated initially with a π-phase shift (''black'') become wider by diffraction and thus arrive as ''gray'' rings at the entrance of the NLM. In our case, the contrast was lowered to $A^2 = 0.88$ [see Fig. 2(b)].

Further insight can be gained by analytically evaluating the transverse velocity of the solitary wave in the model of competing cubic-quintic nonlinearity [Eqs. (8)–(10)]. With the data for A^2, the model shows well-pronounced minimum in the RDSW transverse velocity for powers slightly lower than P_{sol}^{1D} [Fig. 2(b), dashed curve]. The contrast was measured at the end of the nonlinear medium. However, even for fixed input power the RDSW changes its contrast and transverse velocity along the whole length of the medium. In that sense Fig. 2(a) presents the effect of enhancement of the phase shift and the contrast of the RDSW by the saturating nonlinearity in an integral form, accounting for all the propagation in the NLM.

This result, however, does not fully correspond to the monotonic dependence of the transverse velocity on the intensity obtained in the theoretical model [Eq. (6)]. The reason for this difference is that in the theoretical treatment an

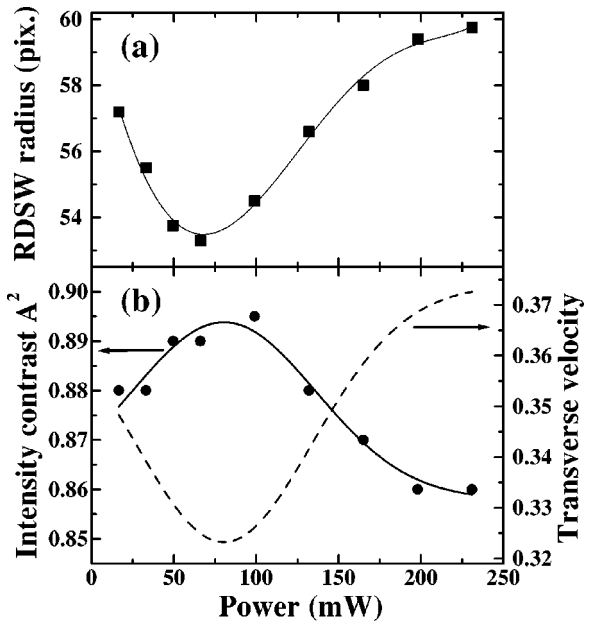

FIG. 2. (a) Power dependence of the RDSW radius after a nonlinear propagation path length $z=8.5$ cm. (b) Power dependence of the RDSW contrast (dots) and estimated transverse velocity (dashed curve) using the model of cubic-quintic nonlinearity ($qI_0=5\times10^{-4}$).

exact quasi-one-dimensional solution is assumed. This means that increase of the background intensity has to be connected to decrease of the RDSW width. In a real experimental situation, however, only the power of the laser could be increased, while the initial width of the dark ring stays the same. It is fixed by the way of reconstruction of the CGH. Therefore, the initial conditions could differ substantially from the exact solutions. For example, the increase of the intensity leads to generation of several coaxial dark rings. In this way, the dynamics of the main ring is influenced by the interaction with the adjacent ring formations. Hence the dependence differs from the monotonic increase predicted theoretically. In order to explain this discrepancy numerical simulations were carried out. The initial radius R_0 was chosen twice as large as the ring width r_0. The free-space evolution of the dark ring before it enters the NLM was also taken into account. In agreement with our measurements, initially ''black'' rings generated by CGHs became ''gray'' after passing four Rayleigh diffraction lengths and reached the estimated contrast $A^2=0.88$. The evolution of the RDSW's radius for different intensities was calculated up to ten nonlinear lengths. The behavior of the RDSW radius in the NLM can be summarized as follows:

(i) For a fixed input intensity in the range of $(0.2–2.2)I_{\mathrm{sol}}^{1D}$ all RDSWs have their minimal radius for propagation distances between $1.5L_{NL}$ and $3L_{NL}$.

(ii) For nonlinear propagation distances shorter than $2L_{NL}$ the gray rings monotonically reduce their radii for increasing intensity (Fig. 3, lowest graph).

(iii) For long propagation distances ($>6L_{NL}$), this tendency is reversed (Fig. 3, upper graph).

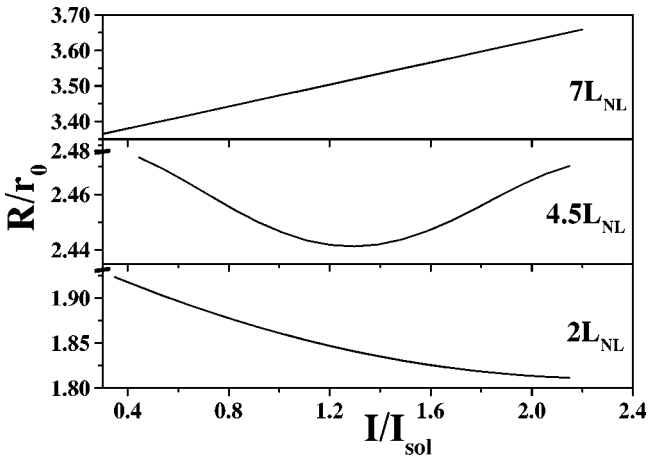

FIG. 3. RDSW radius vs normalized background-beam intensity at three characteristic nonlinear propagation distances. Model parameters $R_0/r_0=2$, $A^2=0.88$, $s=0.4$.

(iv) In between, the radius of the RDSW as a function of the intensity shows a characteristic minimum around $4.5L_{NL}$ (Fig. 3, middle graph). This propagation distance is in reasonable agreement with the NLM length of 8.5 cm corresponding to $4L_{NL}$.

Generally, we found an existence of a minimal radius R_{min} of the RDSW after a characteristic propagation distance, which depends on the initial contrast A^2. The evolution of the contrast itself is influenced by the saturation of the nonlinearity.

C. Influence of the initial free propagation and nonlinearity saturation

It should be pointed out that initially black RDSWs are not likely to be present in a real experiment, at least when generated by holograms. The reason lies in the necessity to select one of the diffracted beams, which requires a certain free-space propagation. After some diffraction is ''accumulated,'' the dark rings with small radii spread out substantially and their contrast decreases. Dark rings with large radii are less affected and they evolve more slowly inside the NLM. Figure 4 is intended to visualize this before and inside the NLM. The coordinate $z=0$ is fixed at the nonlinear interface. Figure 4 also presents a comparison for the nonlinear propagation in Kerr (solid lines) and saturable nonlinearity ($s=0.4$—dashed lines). The general dependence that the nonlinear saturation leads to reduction of the transverse dynamics is clearly visible. The simulation was carried out for $I=I_{\mathrm{sol}}^{1D}$ and for an initial phase jump of π, which is flattened in the course of propagation.

IV. RDSW TRANSVERSE DYNAMICS VS INITIAL PHASE SHIFT

It is important to note that there is no difference whether the phase inside the ring Φ_{in} is bigger or lower than the phase Φ_{out} outside, provided $|\Delta\Phi|=\pi$. Equivalently, there should be no difference in the transverse dynamics of the RDSWs generated by the first positive and first negative dif-

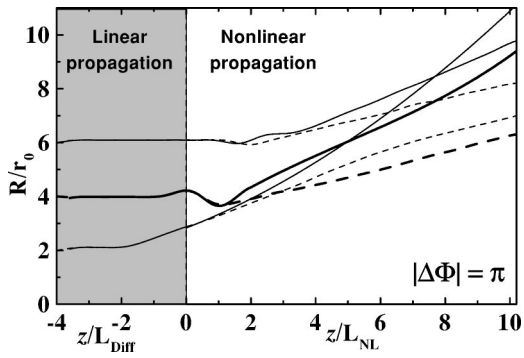

FIG. 4. Diffraction-governed evolution of RDSWs with initial π-phase jumps and three different initial radii over four Rayleigh diffraction lengths followed by nonlinear propagation in a Kerr (solid curves) and saturable Kerr-like medium (dashed curves, $s=0.4$). $I=I_{\mathrm{sol}}^{1D}$. $z=0$, the nonlinear interface.

fraction order beam when a phase jump of π is encoded in the CGHs. This was confirmed experimentally and by numerical simulations. The situation changes when a dark ring (encoded on CGHs) with phase shift smaller than π was generated. The sign of the phase jumps was chosen positive or negative by taking the first positive or the first negative diffraction order. Unfortunately, in the binary CGHs only π/N steps are possible, where one grating period consists of $2N$ elementary stripes. In our case $N=3$ and the gray rings were designed for $|\Delta\Phi|=2\pi/3$.

A. Linear evolution of gray dark rings

First the linear evolution of dark rings with $|\Delta\Phi|=2\pi/3$ was investigated. For this experiment a single-mode He-Ne laser was used. The beam was expanded 3.5 times to reproduce the respective CGH. Figure 5(a) shows the images of the interference of the overlapping first-order diffracted beams and the zeroth order one. It can be seen that the ring with $\Delta\Phi=-2\pi/3$ has smaller radius than the dark ring with an initial π-phase shift. The ring with $\Delta\Phi=2\pi/3$ has the biggest radius, showing that it expands faster even in the linear propagation.

To obtain the dependence of the ring radius as a function of the linear propagation, the CCD array was illuminated directly with the first-order diffracted beam [Fig. 5(b)]. Blank circles denote the dark ring radii for $|\Delta\Phi|=\pi$, the solid circles refer to the ring with encoded phase jump $\Delta\Phi=\pm2\pi/3$. The dark ring radius encoded on the CGH is $R_0=60$ μm. In order to get better spatial resolution, the measurements were repeated by using a lens ($f=4$ cm) imaging different lengths of propagation on the CCD camera, located about 100 cm behind. By varying the lens position we were able to follow the dark ring evolution. The ring radii observed for lens positions from 4 cm to 16 cm are shown in Fig. 5(c). Note that in the two graphs of Figs. 5(b) and 5(c), the ring radius R is denoted in CCD-camera pixels, but these units are not directly comparable because of the different focusing conditions. It is easy to understand the observed tendencies: The diffraction tends to broaden the dark rings and flatten the phase jumps. For $\Phi_{in}<\Phi_{out}$ an effective concave phase front is formed which ''focuses'' the dark ring. In the other diffraction order Φ_{in} appears to be bigger than Φ_{out}. The phase change induced by the diffraction results in an effective convex phase front that increases the dark ring radius. For $|\Delta\Phi|=\pi$, the diffraction influences both first-order beams in the same way, but more weakly.

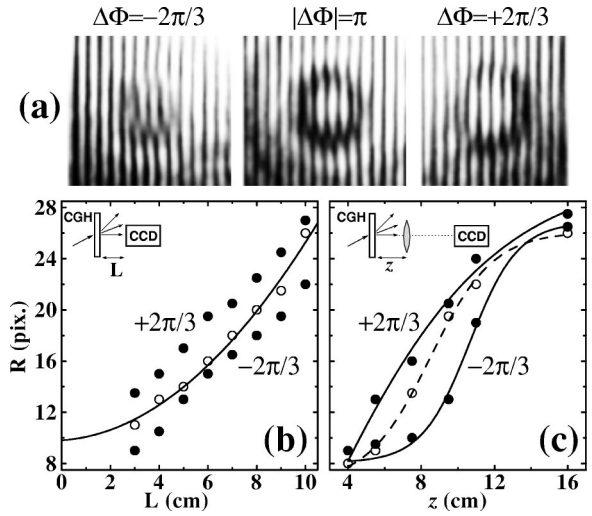

FIG. 5. Linear propagation of ring dark beams: (a) interference patterns indicating different transverse velocities of free propagating, initially gray ($\Delta\Phi=\pm2\pi/3$) and black ($|\Delta\Phi|=\pi$) ring dark beams at $L=5.5$ cm. (b) Ring radii vs CGH-to-CCD-array distance L. (c) The same vs lens-to-CGH distance. Dots, $\pm$ first diffraction order beams; blank circles, initially black dark rings.

B. Nonlinear evolution of initially gray RDSWs

Although the nonlinear regime was analytically analyzed by Kivshar and Yang [6], to the best of our knowledge it has not been investigated experimentally. To clarify the theoretical predictions for an existence of a minimal radius [Eq. (7)], first numerical calculations were conducted. The NLSE was solved numerically by keeping the following parameters close to the experimental values: RDSW radii $R_0/r_0=2,4$, and 6, background-beam intensity $I=I_{\mathrm{sol}}^{1D}$, initial contrast $A^2=0.88$, phase jump $|\Delta\Phi|=0.837\pi$, and saturation of the nonlinearity $s=0.4$. In Fig. 6(a) the corresponding results for the case of a higher phase inside the rings ($\Phi_{in}>\Phi_{out}$) are presented. In this case, the RDSWs start diverging immediately after entering the NLM. The data shown in Fig. 6(b) refer to the case of a lower phase inside the dark ring and higher phase outside ($\Phi_{in}<\Phi_{out}$). The effective concave wave front forces the RDSWs to shrink to a minimum ring diameter. Thereafter, they start to broaden faster. The main tendency is that for broader initial rings the nonlinear propagation required to reach R_{min} is longer. The other general tendency is that the smaller the RDSW diameter, the higher is its transverse dynamic, and also can be clearly seen.

Both tendencies and the influence of the saturation seem to be understood theoretically, but still need experimental confirmation. We performed additional measurements with the experimental setup shown in Fig. 1, in which the telescope is replaced by a single lens ($f=12$ cm) in order to

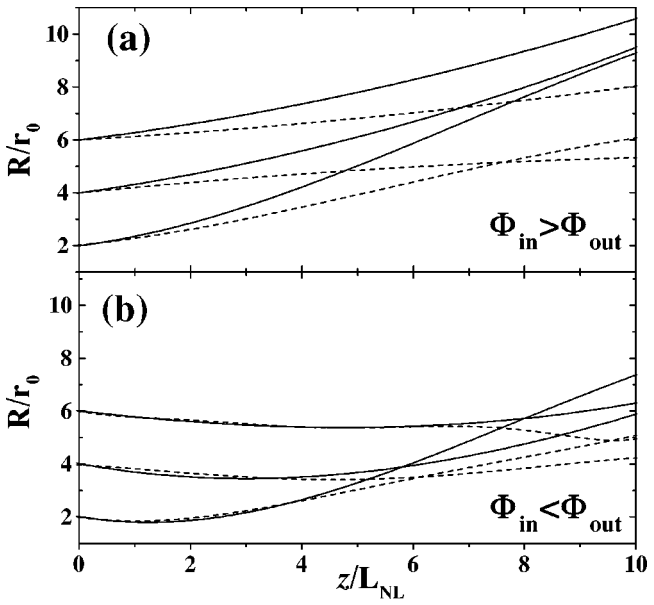

FIG. 6. Nonlinear evolution of initially gray RDSWs in a Kerr (solid curves) and saturable Kerr-like medium (dashed; $s=0.4$) for positive (a) and negative (b) phase shift $\Delta\Phi=\Phi_{in}-\Phi_{out}$. The model parameters correspond to $A^2=0.88$ (i.e., $|\Delta\Phi|=0.837\pi$) and $I=I_{\rm sol}^{1D}$.

focus the beams near the entrance of the NLM. Moderate and strong saturation s can be achieved by raising the absorption α to 0.2 $\rm cm^{-1}$ ($P_{\rm sol}^{1D}=25$ mW; $P_{\rm sat}=40$ mW; $s=0.6$), and 0.4 $\rm cm^{-1}$ ($P_{\rm sol}^{1D}=20$ mW; $P_{\rm sat}=14(\pm5)$ mW; $s\approx1.4$). In order to keep the conditions for both first-order beams as similar as possible, the beam transmitted directly was blocked at the entrance of the NLM and both $\pm$ first order beams were recorded simultaneously. Unfortunately, due to the overlapping of the two background beams, the interaction-free nonlinear propagation path length is limited. The results of the measurements are shown in Fig. 7(a) for moderate and high saturation (host graph and inset, respectively). Blank circles denote "black" RDSWs radii, solid ones RDSW radii for $\Delta\Phi=\pm2\pi/3$. The best results for moderate saturation are achieved with CGHs containing phase dislocations with radii of $R=30$ μm. For high saturation, rings with dislocation radii of 60 μm are used. As seen, after some 5 mm of nonlinear propagation the "gray" RDSWs reach R_{min} and diverge monotonically afterwards. The beam of the other diffraction order and the RDSW generated for $|\Delta\Phi|=\pi$ start diverging from the beginning. The interpolated curves in the figure are intended to guide the eye. The interpolated curves for $z<2$ mm and $z>17$ mm are not shown for an obvious physical reason: As mentioned, the gray RDSWs do not enter the NLM with equal radii and equal (absolute) phase shifts; For larger propagation distances, the saturationlike behavior is caused mainly by interaction with the second copropagating beam. The reduced transverse velocities of the RDSWs for higher saturation are also strongly pronounced. The gray-scale images in Fig. 7(b) show the RDSWs at $z=2$ mm and 8 mm inside the NLM.

By evaluating the data corresponding to the largest RDSWs in our experiment ($R=90$ μm) we observed internal ring splitting at moderate saturation (Fig. 8). Despite their large radii, these RDSWs have nonzero transverse velocity. They broaden and flatten due to the saturation (see Fig. 8, frame at $z=2$ mm) while evolving into gray rings. It seems that such a gray ring can serve as a background on which two coaxial rings can form, subsequently narrow and thus get a high modulation depth for increased propagation distance (Fig. 8, frames at $z=5$ to 17 mm). The mechanism for their formation includes effects from increasing a phase shift and decreasing a transverse velocity due to the saturation of the nonlinearity [16], as well as repulsion between opposite quasi-two-dimensional phase dislocations. We have to note that similar double-ring structure was also observed in the numerical simulations. Example is the propagation of a ring with $R_0=6$ in saturable medium [Fig. 6(b)], where at $z\approx7$ the ring radius is rapidly dropping because of flipping of the total intensity minimum from one ring to the other. The relation of these coaxial rings to the small-amplitude

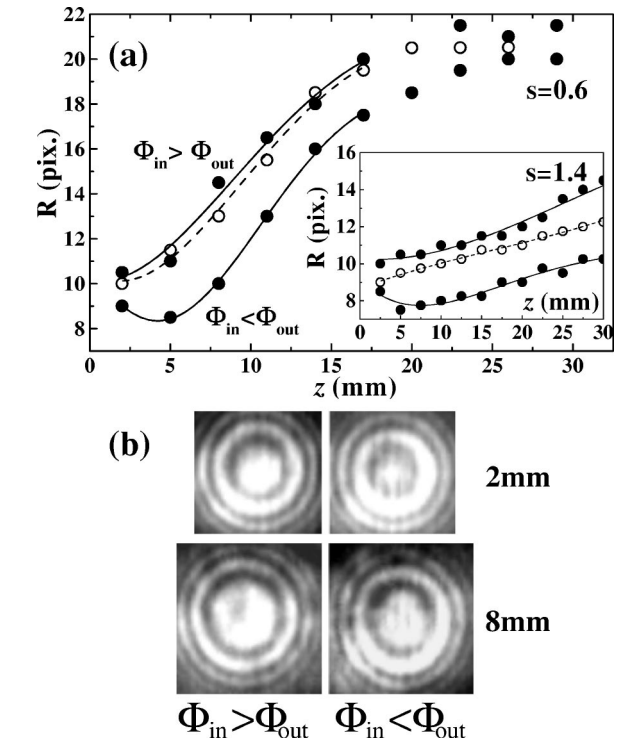

FIG. 7. Nonlinear propagation of RDSWs: (a) evolution of the RDSW radii along the nonlinear medium at moderate (host graph, $s=0.6$) and high saturation (inset, $s=1.4$). Solid and blank circles, initially gray ($|\Delta\Phi|=2\pi/3$) and black ($|\Delta\Phi|=\pi$) RDSWs, respectively. (b) Gray-scale images of RDSWs at $z=2$ mm and 8 mm in a moderately saturated NLM.

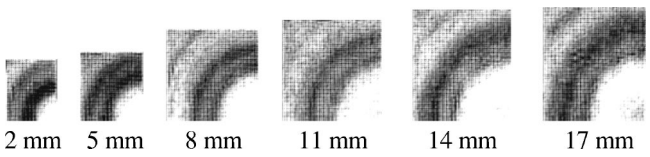

FIG. 8. Gray-scale images showing the development of an internal substructure of a RDSW ($R_0=90$ μm) at moderate saturation.

dark solitary waves described by Frantzeskakis and Malomed [7] still needs to be clarified.

V. CONCLUSION

Experimental investigation of the transverse dynamic of RDSWs propagating in a nonlinear medium is presented and compared to the theoretical predictions [6]. The dynamic depends on the initial conditions for their generation as well as the properties of the medium they propagate in. The parameters determining the initial conditions are the ring radius R_0, the background-beam intensity I_0, and the total phase shift between the inner and outer part of the ring $\Delta\Phi_0$ and their influence was experimentally investigated.

The dependence on the R_0 has been already investigated experimentally earlier [11]. Here we confirmed the general dependence that the transverse velocity of the rings is lower if R_0 is bigger.

The dependence on the I_0 was experimentally investigated in Ref. [9] for rings generated from amplitude modulation only. This method, however, generates rings with very low contrast and low total phase shift. Therefore in Ref. [9] only monotonic increase of the ring radius with the intensity was observed. In the present work the dark rings were generated with higher contrast and we found characteristic regions where the RDSW radius can increase, decrease monotonically or go through a minimum depending on the background-beam intensity.

The dependence of the transverse dynamic on $\Delta\Phi_0$ has not been experimentally investigated to our knowledge. In qualitative agreement with the theoretical predictions [6] we observed a monotonic increase of the dark ring radius for $\Phi_{in} > \Phi_{out}$ and passing through a minimum in the opposite case.

The dynamics of the dark rings was also influenced by the properties of the medium they propagated in. Though an experimental control over the parameters of the medium is harder to obtain, their influence was also pointed out: In the present experimental arrangements the rings experience a free-space propagation which makes it impossible to ensure perfect odd initial conditions (radial phase jumps equal to π and contrast equal to unity). It gives rise to lowering of the ring contrast and total phase shift at the entrance of the nonlinear medium; Inside the NLM the dark rings form RDSWs. Their transverse dynamics is reduced by the saturation of the nonlinearity. This was confirmed numerically by comparing the propagation in Kerr and saturable nonlinear media, and experimentally by comparing the propagation for different values of the saturation parameter.

All of the experimentally obtained results were compared with numerical simulations in the presence of saturation and are in qualitative agreement with the analytical models [6,16].

ACKNOWLEDGMENTS

The authors are pleased to acknowledge highly useful discussions with Yu.S. Kivshar. A.D. would like to thank the Alexander von Humboldt Foundation for financial support and the opportunity to work in the stimulating atmosphere of the Max-Planck-Institut für Quantenoptik (Garching, Germany). This work was also supported by the National Science Foundation of Bulgaria and by the Science Fund of Sofia University.

[1] V. Zakharov and A. Shabat, Zh. Éksp. Teor. Fiz. **64**, 1627 (1973) [Sov. Phys. JETP **37**, 823 (1973)].
[2] Yu.S. Kivshar and B. Luther-Davies, Phys. Rep. **289**, 81 (1997).
[3] G.A. Swartzlander, Jr., D.R. Andersen, J.J. Regan, H. Yin, and A.E. Kaplan, Phys. Rev. Lett. **66**, 1583 (1991).
[4] B. Luther-Davies and Y. Xiaping, Opt. Lett. **17**, 496 (1992).
[5] G.A. Swartzlander, Jr. and C.T. Law, Phys. Rev. Lett. **69**, 2503 (1992); C.T. Law and G.A. Swartzlander, Jr., Opt. Lett. **18**, 586 (1993); V. Tikhonenko, Yu.S. Kivshar, V.V. Steblina, and A.A. Zozulya, J. Opt. Soc. Am. B **15**, 79 (1998).
[6] Yu.S. Kivshar and X. Yang, Phys. Rev. E **50**, R40 (1994); Chaos, Solitons Fractals **4**, 1745 (1994).
[7] D.J. Frantzeskakis and B.A. Malomed, Phys. Lett. A **264**, 179 (1999).
[8] A. Dreischuh, V. Kamenov, and S. Dinev, Appl. Phys. B: Lasers Opt. **B63**, 145 (1996).
[9] S. Baluschev, A. Dreischuh, I. Velchev, S. Dinev, and O. Marazov, Appl. Phys. B: Lasers Opt. **B61**, 121 (1995); Phys. Rev. E **52**, 5517 (1995).
[10] A. Dreischuh, W. Fließer, I. Velchev, S. Dinev, and L. Windholz, Appl. Phys. B: Lasers Opt. **B62**, 139 (1996).
[11] D. Neshev, A. Dreischuh, V. Kamenov, I. Stefanov, S. Dinev, W. Fließer, and L. Windholz, Appl. Phys. B: Lasers Opt. **B64**, 429 (1997).
[12] W.-H. Lee, Prog. Opt. **XVI**, 119 (1978).
[13] C. Creath, in *Temporal Phase Measurement Methods in Interferogram Analysis*, edited by D. Robinson and G. Reid (Institute of Physics, Bristol, 1993), pp. 94–140.
[14] V. Kamenov and A. Dreischuh, Phys. Scr. **55**, 68 (1997).
[15] E.D. Eugenieva and A.A. Dreischuh, Phys. Scr. **58**, 481 (1998).
[16] W. Krolikowski, N. Akhmediev, and B. Luther-Davies, Phys. Rev. E **48**, 3980 (1993).
[17] V. Tikhonenko, J. Christou, B. Luther-Davies, and Yu.S. Kivshar, Opt. Lett. **21**, 1129 (1996).
[18] A.E. Kaplan, Pis'ma Zh. Eksp. Teor. Fiz. **9**, 58 (1969) [JETP Lett. **9**, 33 (1969)]; M.S. Borodin and A.M. Kamuz, *ibid.* **9**, 577 (1969) [*ibid.* **9**, 351 (1969)].